Submitted to ApJ
Preprint typeset using LaTeX style emulateapj v. 11/10/09

DETECTION OF A TRANSITING LOW-DENSITY SUPER-EARTH[1]

Gregory W. Henry[2], Andrew W. Howard[3,4], Geoffrey W. Marcy[3], Debra A. Fischer[5], John Asher Johnson[6]

Submitted to ApJ

ABSTRACT

We present evidence for photometric transits of the low-mass planet HD 97658b across the disk of its host star, an early K dwarf. This planet was previously discovered in radial velocities (RVs) from Keck/HIRES as part of the Eta-Earth Survey. Using photometry from the Automated Photometric Telescopes at Fairborn Observatory, we detected four separate planetary egress events at times predicted from the RV orbit. We measured a transit depth of 1470 ± 260 ppm, a result that should be confirmed and refined with space-based photometry. We also collected additional Keck-HIRES RV measurements that refined the transit ephemeris and planet mass. With an orbital period of 9.4957 ± 0.0022 days, HD 97658b is a close-in planet that had been classified as a 'super-Earth' based on its mass of 6.4 ± 0.7 $M_\oplus$. However, the planet radius of 2.93 ± 0.28 $R_\oplus$ implies a density of $1.40^{+0.53}_{-0.36}$ g cm^{-3} and suggests 'sub-Neptune' status. The low density can be explained by an extended atmosphere of volatiles such as hydrogen, helium, and water. HD 97658b is similar to GJ 1214b in mass, radius, and density, although HD 97658b has a higher equilibrium temperature of 510–720 K. The star HD 97658 ($V = 7.8$, $K = 5.7$) is among the brightest known to host a transiting planet, which will facilitate detailed follow-up measurements.

Subject headings: planetary systems — planets and satellites: formation, interior — stars: individual (HD 97658) — techniques: photometric

1. INTRODUCTION

Transiting planets offer the opportunity to measure the physical properties of other worlds. Measurements of a planet's radius from transit photometry and mass from radial velocities (RVs) or transit time variations (TTVs) yield a planet's density, from which a bulk composition can be inferred or constrained. Transiting planets that orbit bright stars can be studied in great detail. For such planets, primary and secondary eclipse spectroscopy, phase curves, and timing measurements reveal details of the physical composition and evolutionary state. Because most transiting planets are discovered by field surveys of faint stars, such well-studied planets are rare.

Planets of approximately Neptune-size and smaller are among the most sought after because of their great diversity in composition and because they are a step toward studying Earth-size planets. Among the "super-Earths" ($M_p < 10$ $M_\oplus$), measured densities span a factor of nearly 20. The most dense is Kepler-10b, a rock/iron world with a density of 9 g cm^{-3} (Batalha et al. 2011). At the other end of the spectrum, the low density of 0.5 g cm^{-3} for Kepler-11e can only be accounted for with a substantial gas envelope (Lissauer et al. 2011). To date, only two transiting super-Earths (GJ 1214b and 55 Cnc e) have been discovered orbiting nearby stars, although measurements from *Kepler* demonstrate that close-in, sub-Neptune size worlds are more than an order of magnitude more common than Jovian planets (Borucki et al. 2011; Howard et al. 2011a).

The Eta-Earth Survey (Howard et al. 2010) is one of several RV planet searches by the California Planet Search (CPS) group using the HIRES spectrometer (Vogt et al. 1994) on the Keck I telescope. With this survey of 235 nearby, bright GKM dwarfs, we have detected several super-Earth and Neptune-mass planets (e.g. Howard et al. 2009, 2011b,c) and have shown that the planet mass function rises steeply down to 3 $M_\oplus$ (Howard et al. 2010). One of the planets discovered through this survey is HD 97658b, which was estimated to have an orbital period of 9.494 ± 0.005 days and a minimum mass of 8.2 ± 1.2 $M_\oplus$ (Howard et al. 2011c). As with most planets discovered at Keck, we made photometric measurements using the Automated Photometric Telescopes (APTs) at Fairborn Observatory (Eaton et al. 2003). These measurements can detect long-term magnetic cycles (e.g., Henry et al. 1995a), short-term rotational modulation of active regions (e.g., Henry et al. 1995b), and can rule out a spurious RV detection due to rotational modulation of starspot activity (Henry et al. 2000a). For close-in, RV-discovered planets with relatively high transit probabilities and accurate ephemerides, we also search for planetary transits in the light curves after phase-folding to the RV orbit (e.g., Henry et al. 2000b; Sato et al. 2005). In the case of HD 97658, the 318 APT measurements taken over three years were too sparse to place strong limits on transits of the planet (Howard et al. 2011c).

Since the publication of that discovery paper, we have

[1] Based in part on observations obtained at the W. M. Keck Observatory, which is operated jointly by the University of California and the California Institute of Technology. Keck time has been granted by both NASA and the University of California.

[2] Center of Excellence in Information Systems, Tennessee State University, 3500 John A. Merritt Blvd., Box 9501, Nashville, TN 37209, USA; gregory.w.henry@gmail.com
[3] Department of Astronomy, University of California, Berkeley, CA 94720-3411, USA
[4] Space Sciences Laboratory, University of California, Berkeley, CA 94720-7450 USA
[5] Department of Astronomy, Yale University, New Haven, CT 06511, USA
[6] Department of Astrophysics, California Institute of Technology, MC 249-17, Pasadena, CA 91125, USA

undertaken a dedicated campaign to detect or rule out transits of HD 97658b. In this paper we present new, high-cadence photometry demonstrating that HD 97658b transits its host star. In the next section we describe the photometric and RV measurements. We model these measurements in Section 3 to estimate planet properties and conclude in Section 4 with a brief discussion.

2. MEASUREMENTS

2.1. *APT Photometry and Transit Detection*

We made high cadence photometric measurements of HD 97658 with the goal of detecting or ruling out planetary transits, which have a 4% geometric probability. We used two functionally identical APTs, the T12 and the T8, each 0.8 m in diameter and equipped with a two-channel photometer (Henry 1999). These photometers each use two EMI 9124QB bi-alkali photomultiplier tubes to make simultaneous measurements of one star in the Strömgren b and y passbands. We made alternating measurements of HD 97658 and the comparison star HD 99518 ($V = 7.71$, $B - V = 0.343$, F0) and combined the b and y differential magnitudes into $\Delta(b + y)/2$ measurements (Table 1). The uncertainties listed are the standard deviations of the measurements on each night after subtracting a best-fit, box-shaped transit model. These uncertainties are approximately $\sqrt{3}$ higher than for once-per-night monitoring observations with the APTs (as in Howard et al. (2011c)), which are the average of three consecutive differential measurements. The 931 measurements here are from eight separate nights and have a cadence of approximately one differential measurement every 2.5 min. In the analysis that follows, we assumed that the comparison star is constant to within photon statistics and we constructed models based on the relative flux of HD 97658 instead of $\Delta(b + y)/2$ differential magnitudes. In these models and the accompanying figures, we allowed for small photometric offsets from night to night.

Observing conditions were mostly favorable at Fairborn Observatory. The APT observations on each night started just after evening twilight and continued until the star reached airmass 1.9–2.0. The only breaks were a ∼2 hour gap on JD 2,455,650 and a one hour delayed start on JD 2,455,669, both due to clouds. The photometric precision was typical for APT measurements in the spring, although it was slightly lower and more variable from night to night than under the best observing conditions in winter when the atmosphere is most transparent.

The first night of new APT observations was JD 2,455,650, during which Howard et al. (2011c) predicted a transit (assuming edge-on orbital orientation) based on the ephemeris $P = 9.494 \pm 0.005$ days and $T_c = 2{,}455{,}375.01 \pm 0.64$. The photometry (Figure 1, top panel) shows a small discontinuity before and after the gap in continuous coverage due to clouds. This change in brightness of $+1100 \pm 560$ parts per million (ppm) is small and statistically insignificant by itself, but is consistent with HD 97658b being in-transit during the first ∼2 hr that night and out-of-transit afterwards.

With an orbital period of nearly 9.5 days, alternating transits of HD 97658b are visible from a particular site every 19 days at nearly the same time of night. We observed the target on three additional nights with predicted transits (Figure 1, bottom four panels). On JD 2,455,707 we made simultaneous measurements with two APTs, the T12 used for all previous measurements and the T8. We identified photometric discontinuities in each of the light curves at a consistent time each night, approximately Julian Day Fraction (JDF) 0.72. The difference in mean brightness before and after JDF 0.72 is measured with 2–3.5 σ significance in each of the five light curves. Measurements after JDF 0.72 were systematically higher by the amounts listed in Table 2. These offsets can been seen in Figure 1 as the clouds of points shifting higher after JDF 0.72. Collectively, the five light curves show an offset of $+1460 \pm 270$ ppm at JDF 0.72 with 5.5-σ significance. The times of egress measured for each light curve are consist with the prediction from the RV ephemeris to within 1-σ.

We considered two explanations for the photometric discontinuity at JDF 0.72. While it is consistent with the detection of transit egress, a more mundane possibility is an instrumental or atmospheric effect occurring at nearly the same time every night. Hypothetically, such an effect could be related to falling ambient temperature or rising airmass that differentially affects the measurements of HD 97658 and its comparison star. While we have not observed such a spurious photometric offset with APT observations of other stars, we checked for it with this star by observing on four additional nights when tran-

Table 1
Photometric Measurements

JD – 2,440,000	Mag[a]	$\sigma_{\rm Mag}$	Telescope	Note[b]
15650.6106	0.1742	0.0030	T12	T
15650.6124	0.1822	0.0030	T12	T
15650.6141	0.1735	0.0030	T12	T
15650.6175	0.1727	0.0030	T12	T
15650.6191	0.1816	0.0030	T12	T
15650.6208	0.1817	0.0030	T12	T
...				

[a] Photometric measurements are expressed in magnitudes in the $\Delta(b+y)/2$ passband with respect to a comparison star.
[b] Measurements on nights with expected transits are labeled "T" and those on nights when the planet is predicted not to transit are labeled "NT".
[c] This table will be available in its entirety in a machine-readable form in the online journal. A portion is shown here for guidance regarding its form and content.

Table 2
Photometric offset at JDF 0.72

Date(s)	Photometric offset (ppm) at JDF 0.72
Nights with a predicted transit:	
JD 2,455,650	$+1100 \pm 560$
JD 2,455,669	$+2380 \pm 700$
JD 2,455,688	$+1880 \pm 720$
JD 2,455,707 (T12)	$+2320 \pm 640$
JD 2,455,707 (T8)	$+1550 \pm 520$
All in-transit nights	$+1460 \pm 270$
Nights predicted not to transit:	
JD 2,455,693	-590 ± 750
JD 2,455,694	$+880 \pm 690$
JD 2,455,705	$+2010 \pm 1080$
JD 2,455,706	-120 ± 860
All out-of-transit nights	$+390 \pm 400$

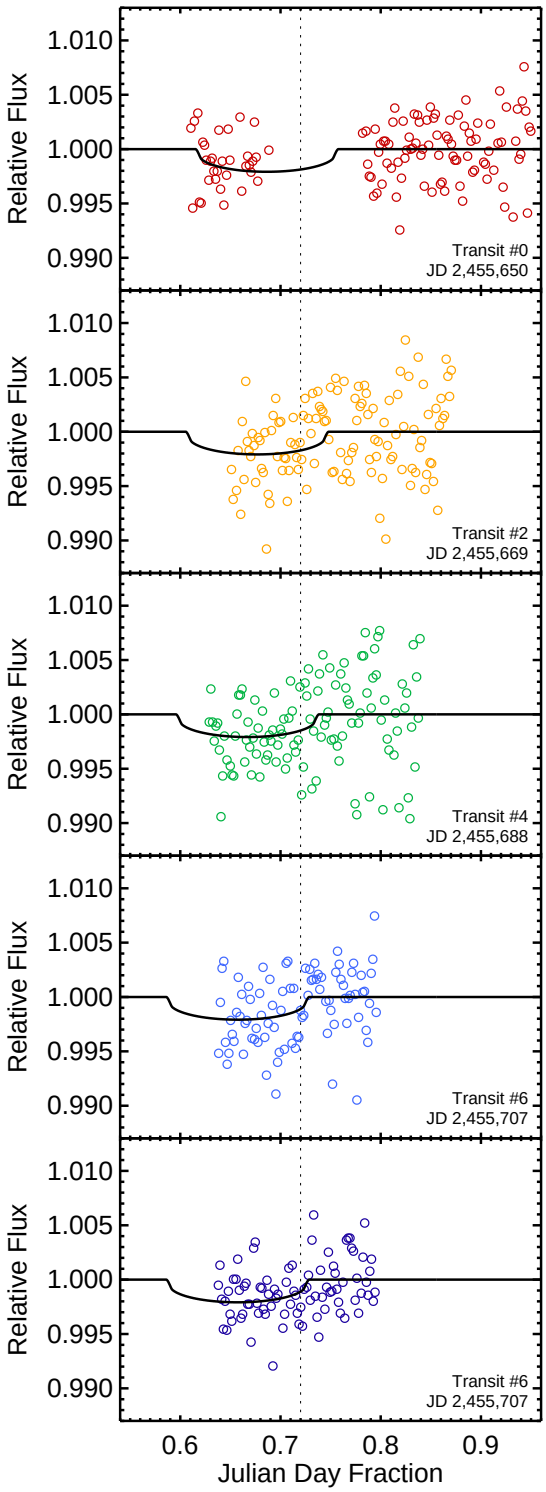

Figure 1. APT photometry of HD 97658 (open circles) from four nights with predicted transits. The dashed vertical line at JDF 0.72 marks the time of night used to compute the photometric offsets that are detected at the 2–3.5-σ level in each light curve (Table 2). The solid lines show the best-fitting limb-darkened transit model (see Section 3). Alternating transits repeat nearly every 19.0 days because the orbital period is 9.4957 ± 0.0022 days. The measurements in these five panels are shown phased with the orbital period in Figure 4. All data are from the T12 APT, except for the bottom panel which are from the T8 APT.

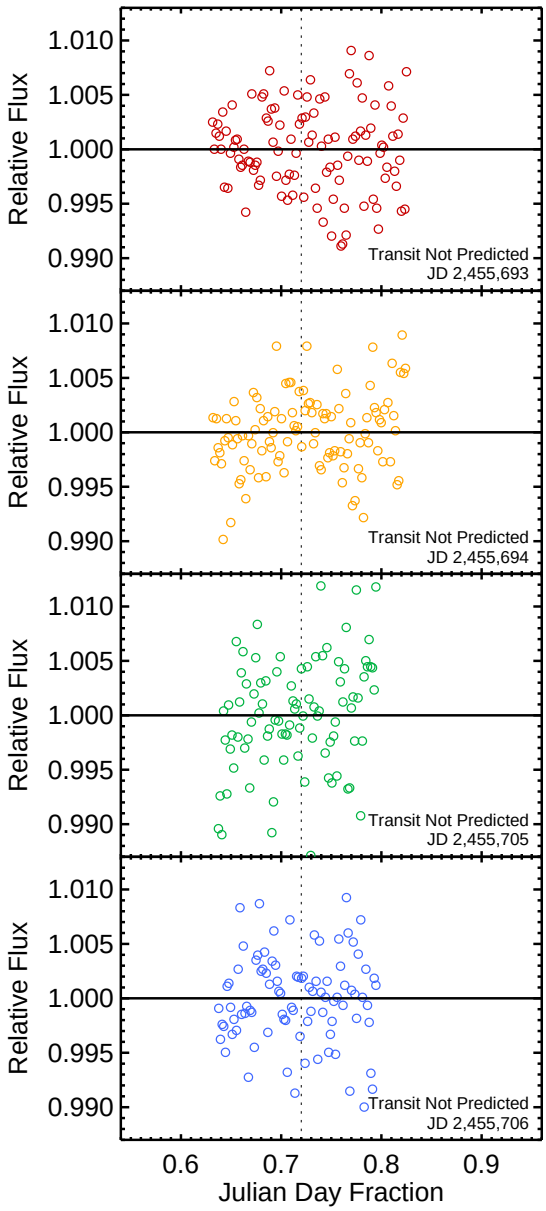

Figure 2. APT photometry of HD 97658 (open circles) from four nights when transits were not predicted. The dashed vertical line at JDF 0.72 marks the time of night used to compute the photometric offsets in each light curve (Table 2). In contrast with the light curves from nights with predicted transits (Figure 1) that show photometric offsets at JDF 0.72 that are consistent with transit egress, these light curves are consistent with a constant photometric model (solid lines). The measurements in these four panels are stacked in Figure 4.

sits were *not* predicted. These measurements (Figure 2) were identical in setup, observing cadence, and comparison star to the observations during which transits were predicted and tentatively detected. As listed in Table 2, measurements before and after JDF 0.72 show no discernible offset. On each night the computed offset at JDF 0.72 is consistent with zero at the 2–σ level. Collectively, the offset of $+390 \pm 400$ ppm in all four light curves is consistent with zero. If the offset was due to an environmental or instrumental affect at a particular time of night it should affect equally the light curves on nights with and without predicted transits, but this was

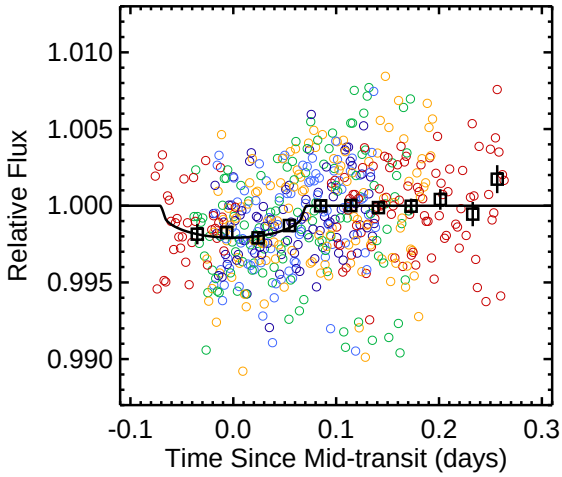

Figure 3. Phased APT photometry of HD 97658 from four nights with predicted transits. The data and symbol colors are the same as in Figure 1. The best-fitting limb-darkened transit model (Section 3) is overplotted by a solid line. Binned measurements (open square symbols) are averaged in 0.03 day intervals. Binned errors (vertical lines) are the uncertainties of the mean of binned measurements.

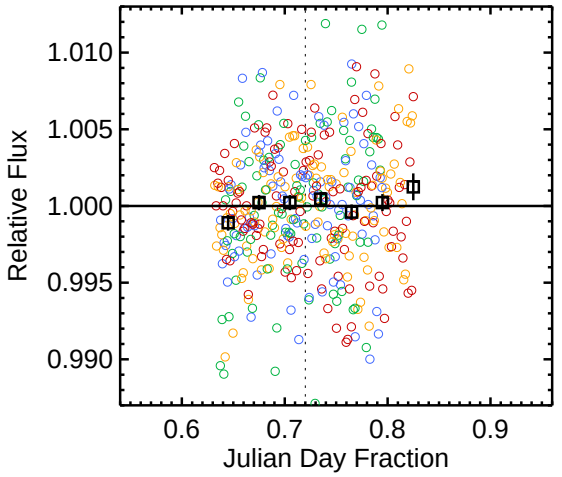

Figure 4. Stacked APT photometry of HD 97658 from four nights when transits were not predicted. The data and symbol colors are the same as in Figure 2. Binned measurements were computed as in Figure 3. If the transit egress features detected on nights with predicted transits (Figures 1 and 3) were an instrumental or atmospheric effect, we would expect a reduction in brightness of ∼1500 ppm for measurements before JDF ≈ 0.72 (dashed vertical line), which is not seen.

not observed. For visual comparison, the phased transit photometry from all four nights is plotted in Figure 3 and the stacked photometry from non-transit nights is shown in Figure 4.

In summary, we detected a small photometric discontinuity in five light curves on nights with predicted transits, but failed to detect the discontinuity on four additional nights of identical observations when the planet was predicted not to transit. We interpret the repeating photometric discontinuities as transit egress.

2.2. *HIRES Spectroscopy*

Howard et al. (2011c) announced the discovery of HD 97658b based on 96 Keck-HIRES RVs. In the past 10 months we made 52 additional measurements with HIRES. We also recorded a series of five "template" spectra without the iodine cell and with the 0.57 arcsec wide "E2" decker. (All other HIRES observations were made with the 0.86 arcsec wide "B5" decker.) This narrow slit permitted a more accurate measurement of the spectrometer PSF during B star observations that bracket the template observations. This in turn reduced systematic errors during deconvolution of the stellar template and improved the accuracy of all RV measurements and the estimation of planetary parameters. We modeled the 148 spectra using standard procedures (Butler et al. 1996) as described in Howard et al. (2011c). The resulting RVs and $S_{\rm HK}$ measurements of the Ca II H & K lines (Isaacson & Fischer 2010) are listed in Table 3.

Table 3
Radial Velocities and $S_{\rm HK}$ values for HD 97658

BJD − 2,440,000	Radial Velocity ($\rm m\,s^{-1}$)	Uncertainty ($\rm m\,s^{-1}$)	$S_{\rm HK}$
13398.04102	8.08	0.67	0.1970
13748.03499	5.50	0.73	0.1900
13806.96227	3.17	0.72	0.1870
14085.15886	−4.16	0.80	0.1785
14246.87901	−1.62	0.73	0.1760
...			

[a] This table will be available in its entirety in a machine-readable form in the online journal. A portion is shown here for guidance regarding its form and content.

In Section 3 we will fit the Keck RVs and APT photometry with a self-consistent model. Prior to this we checked the ephemeris of Howard et al. (2011c) by fitting the RVs to a single-planet Keplerian model with no constraints from the photometry. We first verified the single-planet solution by searching over a wide range of orbital periods using the partially-linearized technique of Wright & Howard (2009). To quantify the best-fit solution, we used a Markov Chain Monte Carlo (MCMC) algorithm (Ford 2005, 2006) and report the median, 84.1%, and 15.9% levels of the marginalized posterior distributions. The likelihood was taken to be $e^{-\chi^2/2}$, where χ^2 is the usual sum of the standardized residuals between the observed and calculated RVs. We adopted a Gregory eccentricity prior (Gregory & Fischer 2010) and non-informative priors on other parameters. We excluded three outliers that were $\geq$7 $\rm m\,s^{-1}$ from the best-fit model that has a residual RMS of 2.31 $\rm m\,s^{-1}$ with the remaining measurements. Our analysis reveals a slightly lower mass of 6.5 ± 0.7 $M_\oplus$ and a more accurate transit ephemeris ($P = 9.4922 \pm 0.0025$, T_c = JD 2,455,650.29 ± 0.43) than in Howard et al. (2011c). The MCMC analysis is consistent with a circular orbit and excludes $e > 0.29$ with 95% confidence.

We also used the five new, higher resolution iodine-free spectra from Keck-HIRES to check the stellar parameters reported in Howard et al. (2011c). An accurate estimate of the stellar radius, $R_\star$, is particularly important as errors propagate directly to the planet radius, R_p. As in Howard et al. (2011c), we used Spectroscopy Made Easy (SME; Valenti & Piskunov 1996; Valenti & Fischer 2005) to model the spectra. We further constrained surface gravity using Yonsei-Yale ($\rm Y^2$) stellar structure models (Demarque et al. 2004) and revised *Hipparcos* parallaxes (van Leeuwen 2007) using the iterative method of

Table 4
Stellar and Planetary Properties

Parameter	Value	Source
Photometric properties		
M_V (mag)	6.27 ± 0.10	Tycho + Hipparcos
$B-V$ (mag)	0.843 ± 0.022	Tycho
V (mag)	7.762 ± 0.012	Tycho
J (mag)	6.203 ± 0.023	2MASS
H (mag)	5.821 ± 0.017	2MASS
K (mag)	5.734 ± 0.018	2MASS
Stellar properties		
MK spectral type	K1 V	Gray et al. (2003)
Distance (pc)	21.1 ± 0.33	Hipparcos
Effective temperature, $T_{\rm eff}$ (K)	5119 ± 44	SME [a]
Surface gravity, $\log g$	4.52 ± 0.06	SME
Iron abundance, [Fe/H]	-0.30 ± 0.03	SME
Projected rotational velocity, $v_{\rm rot} \sin i_{\rm rot}$ ($\rm km\,s^{-1}$)	0.48 ± 0.50	SME
Rotational velocity, $v_{\rm rot}$ ($\rm km\,s^{-1}$)	0.92 ± 0.05	$S_{\rm HK}$ time series
Rotational period, $P_{\rm rot}$ (days)	38.5 ± 1.0	$S_{\rm HK}$ time series
Luminosity, $L_\star$ ($L_\odot$)	0.30 ± 0.02	$\rm Y^2$+ SME [b]
Mass, $M_\star$ ($M_\odot$)	0.75 ± 0.02	$\rm Y^2$+ SME
Radius, $R_\star$ ($R_\odot$)	0.70 ± 0.02	$\rm Y^2$+ SME
Age (Gyr)	7.0 ± 4.4	$\rm Y^2$+ SME
Age (Gyr)	5.8 ± 1.0	$\log R'_{\rm HK}$ calibration
Age (Gyr)	6.1 ± 0.7	$P_{\rm rot}$ calibration
Orbital and photometric properties		
Orbital period, P (days)	9.4957 ± 0.0022	RV + photometry model [c]
Time of transit, T_c	JD 2,455,650.681 $\pm$ 0.012	RV + photometry model
Eccentricity, e	$0.13^{+0.07}_{-0.06}$	RV + photometry model
Longitude of pericenter, ω (deg)	192^{+46}_{-60}	RV + photometry model
$e \cos \omega$	-0.09 ± 0.06	RV + photometry model
$e \sin \omega$	-0.02 ± 0.10	RV + photometry model
Doppler semi-amplitude, K ($\rm m\,s^{-1}$)	2.36 ± 0.27	RV + photometry model
Transit depth, $(R_p/R_\star)^2$ (ppm)	1470 ± 260	RV + photometry model
Scaled planet radius, $R_p/R_\star$	0.0384 ± 0.0034	RV + photometry model
Scaled semi-major axis, $a/R_\star$	$20.7^{+3.0}_{-1.6}$	RV + photometry model
Derived properties		
Planet mass, M_p ($M_\oplus$)	6.4 ± 0.7	RV + photometry model
Planet radius, R_p ($R_\oplus$)	2.93 ± 0.28	RV + photometry model
Planet density, ρ_p ($\rm g\,cm^{-3}$)	$1.40^{+0.53}_{-0.36}$	RV + photometry model
Orbital inclination, i (deg)	90.0 ± 1.0	RV + photometry model
Impact parameter, b	$0.29^{+0.24}_{-0.20}$	RV + photometry model
Orbital distance, a (AU)	0.0797 ± 0.0007	RV + photometry model
Equilibrium temperature, $T_{\rm eq}$ (K), for A = 0–0.75	510–720	RV + photometry model

[a] SME = "Spectroscopy Made Easy" package for the analysis of high-resolution spectra. These parameters rely primarily on SME, but have a small dependence on an iterative analysis incorporating an isochrone search (Valenti et al. 2009).
[b] $\rm Y^2$+ SME = Based on the Yonsei-Yale isochrones with iterative refinements from SME.
[c] Simultaneous model of Keck RVs spanning seven years and APT photometry from four nights with predicted transits. Some parameters are constrained primarily by one dataset. See Section 3 for details.

Valenti et al. (2009). The stellar parameters listed in Table 4 are consistent to within 2-σ of the parameters in Howard et al. (2011c). We checked that the standard deviations of the stellar parameters separately estimated from the five spectra are smaller than the standard SME errors (Valenti & Fischer 2005) listed in Table 4, which encompass additional sources of uncertainty. For reference, Table 4 also lists the spectral type, distance from Hipparcos (van Leeuwen 2007), optical photometry from Tycho (Perryman et al. 1997; Bessell 2000), and near-IR photometry from 2MASS (Cutri et al. 2003).

In addition, we used the HIRES spectra to measure the stellar rotation period. In Howard et al. (2011c) we were unable to detect rotational modulation of stellar surface features in three years of APT photometry. However, using the $S_{\rm HK}$ time series based on Ca II H & K measurements from HIRES spectra (Table 3; Isaacson & Fischer 2010) we detected two sources of variability. The first is a long-term magnetic activity cycle with a period of at least 6 years (the span of our HIRES measurements). We subtracted off this long term signal and examined only the high-cadence $S_{\rm HK}$ time series from JD 2,451,000 onward (the past $\sim$2 years). A periodogram of these data reveal a strong peak at 38.5 ± 1.0 days, which we interpret as the stellar rotation period. This period implies an age of 6.1 ± 0.7 Gyr using the Barnes (2007) relation with refinement by Mamajek & Hillenbrand (2008). This is consistent with other ages estimates (see Table 4) based on $\log R'_{\rm HK}$ calibration (Mamajek & Hillenbrand 2008) and isochrone-SME fitting (Valenti & Fischer 2005; Valenti et al. 2009).

3. ANALYSIS AND PLANET PROPERTIES

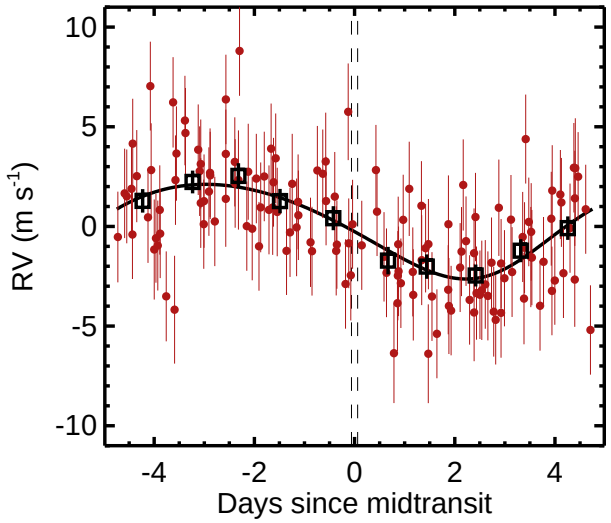

Figure 5. RV measurements (red filled circles) phased to the best-fit orbital period and phase of the joint RV-photometric model (Section 3). The best-fit model is overplotted as a black line. RV measurements are binned in 0.1 phase intervals (black open squares) and have an RMS to the model of 0.33 $\mathrm{m\,s^{-1}}$. Dashed vertical lines mark transit ingress and egress.

Having established that transits were detected in the previous section, we now estimate planet properties by simultaneously modeling the APT photometry as a limb-darkened transit light curve and the Keck RVs as a single-planet Keplerian function. We adopted the non-linear limb darkening model and code by Mandel & Agol (2002). The limb darkening coefficients, $c_{1-4} = \{0.6809, -0.7372, 1.4522, -0.5040\}$, are the mean of the b and y passband coefficients for Phoenix stellar atmosphere models of the nearest grid point ($T_{\rm eff} = 5200$ K, $\log g = 4.5$, [Fe/H]$= 0.0$, $V_T = 2.0$) of stellar parameters (Claret 2000). Because of the small S/N for the transit depth, we fixed the limb darkening prescription, although comparison with the transit depth measured using a box-shaped model suggests that this assumption does not dominate the error budget.

In our model the Keplerian orbital parameters P, T_c, $e\cos\omega$, and $e\sin\omega$ were self-consistently constrained by both datasets. The remaining parameters were constrained by only the RVs (Doppler semi-amplitude K and RV offset γ) or the photometry ($R_p/R_\star$, $a/R_\star$, orbital inclination i, and an offset for photometry on every night with a predicted transit). We explored the parameter uncertainties and correlations with an MCMC algorithm (Ford 2005, 2006) and report the median, 84.1%, and 15.9% levels of the marginalized posterior distributions of the planet parameters (Table 4). To compute the planet's mass and radius we adopted the stellar mass and radius derived from SME analysis of five HIRES spectra (Table 4). The best-fit photometric and RV models are shown in Figures 3 and 5.

The key results are that the transit is detected with a fractional depth uncertainty of 5.5 and that the radius of 2.93 ± 0.28 $R_\oplus$ is large for a planet of mass of 6.4 ± 0.7 $M_\oplus$, implying a low density of $1.40^{+0.53}_{-0.36}$g cm^{-3}. The transit ephemeris from this joint analysis is consistent with but substantially more precise than the ephemeris from the RV-only model.

4. DISCUSSION

We have detected four transits of the planet HD 97658b using APT photometry. One of the transits was observed by two telescopes. Because of the nearly 9.5 day orbital period of this RV-discovered planet, alternating transits repeat at a given site at nearly the same time of night every 19 days. As a result, we detected egress but not ingress of four alternating transits. In each light curve egress is detected with 2 to 3.5-σ confidence, but collectively these add to give 5.5-σ confidence in the transit detection. We also observed the star with the same setup on four nights when transits were not predicted. Non-detection of egress-like features on these nights confirmed the transit detections on the nights when they were predicted.

From the APT photometry we measured $(R_p/R_\star)^2 = 1470 \pm 260$ ppm from which we inferred a planet radius of 2.93 ± 0.28 $R_\oplus$. Combined with the revised planet mass of 6.4 ± 0.7 $M_\oplus$, the density is $1.40^{+0.53}_{-0.36}$ g cm^{-3}. The low density suggests that this 'super-Earth' (based on a mass threshold of $M \sin i < 10$ $M_\oplus$) is more appropriately described as a 'sub-Neptune'.

The mass and radius of HD 97658b do not uniquely specify a composition. We can however rule out purely gaseous (hydrogen/helium) as well as solid (ice/rock/iron), atmosphere-free planets using the Fortney et al. (2007b) models. As shown in the mass-radius diagram in Figure 6, HD 97658b has a lower bulk density than all solid planet composition contours. An atmosphere must contribute substantially to the radius of this planet to explain the low density. Such an atmosphere could have been captured from nebular gas, degassed during accretion, and/or degassed during subsequent tectonic activity (Elkins-Tanton & Seager 2008; Rogers et al. 2011). The gas component need not dominate the mass fraction, however. Adams et al. (2008) found that adding a H/He gas envelope equivalent to 0.2–20% of the mass of a solid 5 $M_\oplus$ exoplanet increases the radius 8–110% above the gas-free value. Atmospheres dominated by heavier molecules such as H_2O and N_2 (as on Earth) would swell the planet less for the same atmospheric mass because of the higher mean molecular weight and reduced scale height.

HD 97658b and GJ 1214b have strikingly similar bulk physical properties. The discovery mass of 6.55 $\pm$ 0.98 $M_\oplus$ and radius of 2.68 $\pm$ 0.13 $R_\oplus$ for GJ 1214 (Charbonneau et al. 2009) are within 1–σ of the values we measured for HD 97658b (Table 4). This comparison is somewhat complicated by recent photometry by Carter et al. (2011) which implies a planet radius of either 2.65 ± 0.09 $R_\oplus$ or 2.27 ± 0.08 $R_\oplus$, depending on systematic errors from starspot dilution. Nevertheless, it is instructive to consider models constructed for GJ 1214b that assume a radius and mass similar to HD 97658b, keeping in mind that HD 97658b has an equilibrium temperature of 510–720 K for albedos $A = 0$–0.75, compared with $T_{\rm eq} = 393$–555 K for GJ 1214b.

Rogers et al. (2011) considered three possible sources for the atmosphere of GJ 1214b, which is required to explain its radius and mass. First, the gas could have been H/He accreted from the protoplanetary nebula. Such an atmosphere would only be 0.01–5% of the planet mass, depending on the relative fractions of iron, silicates, and

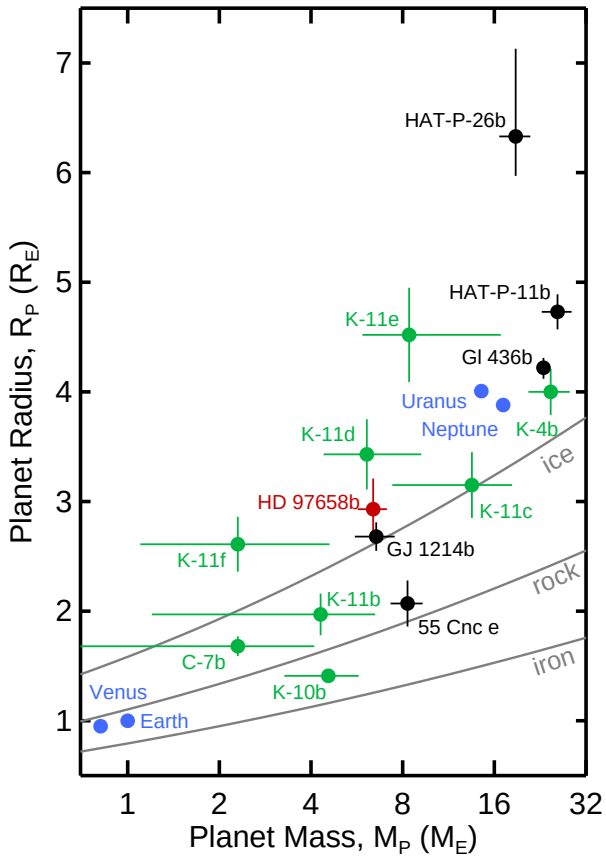

Figure 6. Planet radius versus mass for planets of approximately Earth-size to Neptune-size. HD 97658b is shown in red, other ground-based discoveries in black, Kepler/CoRoT discoveries in green, and Solar System planets in blue. Solid gray lines mark solid planet contours of pure ice (H_20), pure rock (Mg_2SiO_4) , and pure iron (Fe) using the Fortney et al. (2007a,b) models. The planets and measurements in this figure are: Kepler-4b = "K-4b" (Borucki et al. 2010); Kepler-10b = "K-10b" (Batalha et al. 2011); Kepler-11b–f = "K-11b–f" (Lissauer et al. 2011); CoRoT-7b = "C-7b" (we adopt Léger et al. (2009) for R_p and Pont et al. (2011) for M_p, but acknowledge that Hatzes et al. (2011) and others measured a higher mass using the same RVs); 55 Cnc e – an average of Winn et al. (2011) and Demory et al. (2011) for R_p and M_p derived from Fischer et al. (2008); Gl 436b (Maness et al. 2007; Gillon et al. 2007); GJ 1214b (Charbonneau et al. 2009); HAT-P-11b (Bakos et al. 2010); HAT-P-26b (Hartman et al. 2011).

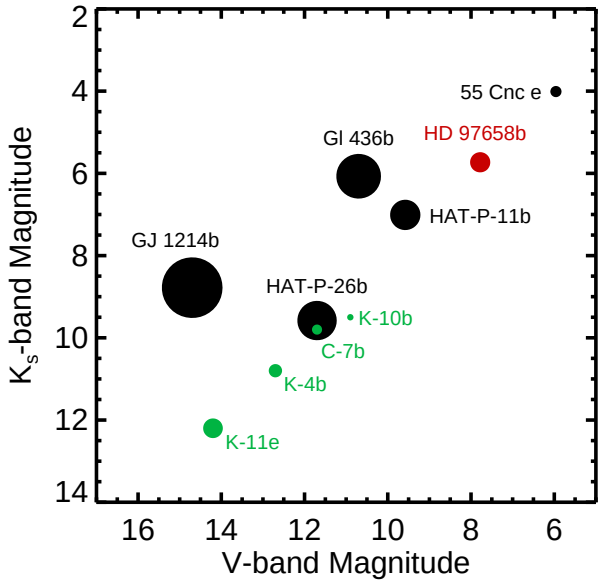

Figure 7. Three attributes of follow-up suitability for transiting planets. Host star K_s-band magnitude (2.15 μm) is plotted against V-band magnitude (0.55 μm) with symbol area proportional to transit depth. Planets that produce deep transits of bright stars are the most suitable for detailed follow-up with ground- and space-based observatories. Only the transiting low-mass extrasolar planets in Figure 6 are shown. For the multi-transiting system Kepler-11, the deepest transit (planet "e") is shown. Kepler and CoRoT planets are abbreviated with "K" and "C" prefixes.

water ice in the interior. Second, GJ 1214b could be a water world with sublimated ices dominating the gas layer. Such a planet would be at least 47% H_2O by mass, which is plausible for a planet of comet-like composition formed beyond the ice line (Selsis et al. 2007). Third, if a nascent atmosphere was lost, a secondary atmosphere could have outgassed from the rocky interior. Such an atmosphere would likely have low He content due to poor sequestration in silicates.

Distinguishing between model atmospheres dominated by H/He, H_2O, and CO_2 is in principle possible given current measurement precision (Miller-Ricci & Fortney 2010). However, measurements of GJ 1214b across the visible and near-IR have not revealed a coherent picture. Bean et al. (2010) measured a flat, featureless spectrum between 780 and 100 nm, which is inconsistent with a cloud-less, H-dominated atmosphere. *Spitzer* measurements at 3.6 and 4.5 μm by Désert et al. (2011) are also inconsistent with an H-dominated atmosphere and favor, instead, a metal-rich (possibly H_2O-rich) atmosphere. Croll et al. (2011) cast doubt on this picture by measuring different planet radii at 1.25 μm and 2.15 μm, implying an atmospheric absorption feature consistent with an H-dominated planet. More complicated models involving clouds, hazes, and non-equilibrium chemistry are compatible with these primary transit measurements, although additional measurements sensitive to H_2O and CH_4 features will offer important constraints (Miller-Ricci Kempton et al. 2011).

We encourage follow-up measurements of HD 97658b to confirm the transiting geometry, more accurately measure R_p, and assess atmospheric composition. HD 97658b has several attributes that make it attractive for detailed follow-up studies. As shown in Figure 7, HD 97658 is the second brightest transiting super-Earth host at visible (V-band) and near-IR (K_s-band) wavelengths, after 55 Cnc e (Winn et al. 2011; Demory et al. 2011). Transits are a factor of four deeper than for 55 Cnc e, but a factor of eight shallower than for GJ 1214b. In addition, HD 97658 is bright and close enough for a precise interferometric measurement of $R_\star$ (e.g., von Braun et al. 2011), which will improve the precision of the R_p measurement. A measurement of the spin-orbit angle, which would offer clues to the formation and migration history of this planet, will be challenging but potentially feasible. We predict a Rossiter-McLaughlin amplitude of $\sim$0.9 m s^{-1} for $v_{\rm rot} \sin i_{\rm rot} \approx v_{\rm rot} = 0.92 \pm 0.05$ km s^{-1} .

We thank the many observers who contributed to the

measurements reported here. We gratefully acknowledge the efforts and dedication of the Keck Observatory staff, especially Scott Dahm, Hien Tran, and Grant Hill for support of HIRES and Greg Wirth for support of remote observing. We thank Heather Knutson, Josh Winn, and Jonathan Fortney for helpful discussions.

We are grateful to the time assignment committees of the University of California and NASA. G. W. H. acknowledges support from NASA, NSF, Tennessee State University, and the State of Tennessee through its Centers of Excellence program. G. W. M. acknowledges NASA grant NNX06AH52G. D. A. F. acknowledges support from NSF grant AST-1036283 and NASA grant NNX08AF42G. This work made use of the SIMBAD database (operated at CDS, Strasbourg, France), NASA's Astrophysics Data System Bibliographic Services, and the NASA Star and Exoplanet Database (NStED). Finally, the authors wish to extend special thanks to those of Hawai'ian ancestry on whose sacred mountain of Mauna Kea we are privileged to be guests. Without their generous hospitality, the Keck observations presented herein would not have been possible.

REFERENCES

Adams, E. R., Seager, S., & Elkins-Tanton, L. 2008, ApJ, 673, 1160
Bakos, G. Á., et al. 2010, ApJ, 710, 1724
Barnes, S. A. 2007, ApJ, 669, 1167
Batalha, N. M., et al. 2011, ApJ, 729, 27
Bean, J. L., Miller-Ricci Kempton, E., & Homeier, D. 2010, Nature, 468, 669
Bessell, M. S. 2000, PASP, 112, 961
Borucki, W. J., et al. 2010, ApJ, 713, L126
—. 2011, ApJ accepted, arXiv:1102.0541
Butler, R. P., Marcy, G. W., Williams, E., McCarthy, C., Dosanjh, P., & Vogt, S. S. 1996, PASP, 108, 500
Carter, J. A., Winn, J. N., Holman, M. J., Fabrycky, D., Berta, Z. K., Burke, C. J., & Nutzman, P. 2011, ApJ, 730, 82
Charbonneau, D., et al. 2009, Nature, 462, 891
Claret, A. 2000, A&A, 363, 1081
Croll, B., Albert, L., Jayawardhana, R., Miller-Ricci Kempton, E., Fortney, J. J., Murray, N., & Neilson, H. 2011, ApJ, 736, 78
Cutri, R. M., et al. 2003, The IRSA 2MASS All-Sky Point Source Catalog, NASA/IPAC Infrared Science Archive, http://irsa.ipac.caltech.edu/applications/Gator
Demarque, P., Woo, J., Kim, Y., & Yi, S. K. 2004, ApJS, 155, 667
Demory, B. ., et al. 2011, arXiv:1105.0415
Désert, J.-M., et al. 2011, ApJ, 731, L40
Eaton, J. A., Henry, G. W., & Fekel, F. C. 2003, in Astrophysics and Space Science Library, Vol. 288, Astrophysics and Space Science Library, ed. T. D. Oswalt, 189
Elkins-Tanton, L. T., & Seager, S. 2008, ApJ, 685, 1237
Fischer, D. A., et al. 2008, ApJ, 675, 790
Ford, E. B. 2005, AJ, 129, 1706
—. 2006, ApJ, 642, 505
Fortney, J. J., Marley, M. S., & Barnes, J. W. 2007a, ApJ, 668, 1267
—. 2007b, ApJ, 659, 1661
Gillon, M., et al. 2007, A&A, 472, L13
Gray, R. O., Corbally, C. J., Garrison, R. F., McFadden, M. T., & Robinson, P. E. 2003, AJ, 126, 2048
Gregory, P. C., & Fischer, D. A. 2010, MNRAS, 403, 731
Hartman, J. D., et al. 2011, ApJ, 728, 138
Hatzes, A. P., et al. 2011, arXiv:1105.3372
Henry, G. W. 1999, PASP, 111, 845
Henry, G. W., Baliunas, S. L., Donahue, R. A., Fekel, F. C., & Soon, W. 2000a, ApJ, 531, 415
Henry, G. W., Eaton, J. A., Hamer, J., & Hall, D. S. 1995a, ApJS, 97, 513
Henry, G. W., Fekel, F. C., & Hall, D. S. 1995b, AJ, 110, 2926
Henry, G. W., Marcy, G. W., Butler, R. P., & Vogt, S. S. 2000b, ApJ, 529, L41
Howard, A. W., et al. 2009, ApJ, 696, 75
—. 2010, Science, 330, 653
—. 2011a, arXiv:1103.2541
—. 2011b, ApJ, 726, 73
—. 2011c, ApJ, 730, 10
Isaacson, H., & Fischer, D. 2010, ApJ, 725, 875
Léger, A., et al. 2009, A&A, 506, 287
Lissauer, J. J., et al. 2011, Nature, 470, 53
Mamajek, E. E., & Hillenbrand, L. A. 2008, ApJ, 687, 1264
Mandel, K., & Agol, E. 2002, ApJ, 580, L171
Maness, H. L., Marcy, G. W., Ford, E. B., Hauschildt, P. H., Shreve, A. T., Basri, G. B., Butler, R. P., & Vogt, S. S. 2007, PASP, 119, 90
Miller-Ricci, E., & Fortney, J. J. 2010, ApJ, 716, L74
Miller-Ricci Kempton, E., Zahnle, K., & Fortney, J. J. 2011, arXiv:1104.5477
Perryman, M. A. C., et al. 1997, A&A, 323, L49
Pont, F., Aigrain, S., & Zucker, S. 2011, MNRAS, 411, 1953
Rogers, L. A., Bodenheimer, P., Lissauer, J. J., & Seager, S. 2011, arXiv:1106.2807
Sato, B., et al. 2005, ApJ, 633, 465
Selsis, F., et al. 2007, Icarus, 191, 453
Valenti, J. A., & Fischer, D. A. 2005, ApJS, 159, 141
Valenti, J. A., & Piskunov, N. 1996, A&AS, 118, 595
Valenti, J. A., et al. 2009, ApJ, 702, 989
van Leeuwen, F. 2007, A&A, 474, 653
Vogt, S. S., et al. 1994, in Proc. SPIE Instrumentation in Astronomy VIII, David L. Crawford; Eric R. Craine; Eds., Vol. 2198, p. 362
von Braun, K., et al. 2011, arXiv:1106.1152
Winn, J. N., et al. 2011, arXiv:1104.5230
Wright, J. T., & Howard, A. W. 2009, ApJS, 182, 205